RSC Advances

This is an *Accepted Manuscript*, which has been through the Royal Society of Chemistry peer review process and has been accepted for publication.

Accepted Manuscripts are published online shortly after acceptance, before technical editing, formatting and proof reading. Using this free service, authors can make their results available to the community, in citable form, before we publish the edited article. This *Accepted Manuscript* will be replaced by the edited, formatted and paginated article as soon as this is available.

You can find more information about *Accepted Manuscripts* in the **Information for Authors**.

Journal Name

ARTICLE

Controlling carriers trapping and relaxation with a dipole field in an organic field-effect device

Yu-Fu Wang,[a] Min-Ruei Tsai,[a] Po-Yang Wang,[b] Chin-Yang Lin,[a] Horng-Long Cheng,[a] Fu-Ching Tang,[c] Steve Lien-Chung Hsu,[d] Jim Hsu[b] and Wei-Yang Chou*[,a]

A series of polyimides (PIs) containing different weight ratios of polar piperazinyl and cholesterol side chains, denoted as PCPI, was synthesized in this study. These PIs were used as gate dielectrics of *n*-type organic field-effect transistors (OFETs) and as electrets of photo-assisted organic memories. The thermal properties of the PI/PCPI composite films were improved by increasing the spatial distribution of the PCPI molecules to form a thermally stable dielectric film. The performances of OFETs, as PIs were used as gate dielectrics, were gradually enhanced by increasing the mixture ratios of the PCPI molecules. A dipole field, which originated from the PCPI molecules into the OFETs, was introduced to observe the special phenomenon of output current growth under a long operation time. The application of these superior transistors with PCPI- and PI-mixed electrets to the field of organic memory resulted in a photo-assisted memory window of more than 38 V. The mechanisms of the carriers trapped in and released from the PI electrets were elucidated. Results showed that our devices possess excellent stability for OFETs and an extra-large memory window for organic memory devices.

1. Introduction

Organic material-based electronics have been extensively investigated over the past decade because of their low manufacturing cost, low temperature process, and flexibility.[1,2] The electrical properties of organic field-effect transistors (OFETs) are generally determined by the interface properties between semiconductors and dielectric layers. Several unfavorable factors, such as interface carrier trap-induced electrical hysteresis in the transfer properties of transistors, attenuated charge carrier mobility caused by oxygen doping into semiconductor layers, and carrier scattering at crystal boundaries, cause the undesirable electrical performance of OFETs.[3,4] These issues are particularly serious for *n*-type OFETs. Accordingly, *n*-type OFETs with high electrical stability are needed in high-performance complementary metal–oxide–semiconductor devices within the integration circuit. To achieve highly stable OFETs and thereby overcome the aforementioned issues, we used a series of polyimide (PI)-based polymer dielectrics with quasi-permanent charges or

immobile electrical dipoles in *n*-type OFETs. PIs are notable dielectric materials because of their excellent mechanical properties, high thermal stability, and flexible molecular structure.[5,6] OFET-based memory devices, which insert charge storable electret layers between semiconductors and insulator layers, have been extensively investigated.[7] Kim et al. demonstrated that the electrical and memory properties of pentacene-based organic memory transistors are affected by the surface polarization degree of polymer electrets.[8] The polarity effects of charge storable electrets on OFETs or memory devices have also been proposed.[9] Moreover, the electrical stability and field-effect mobility of *n*-type organic memory transistors are restricted by the slow relaxation of trapped charges at the interface or semiconductor bulks; this phenomenon leads to a relatively low carrier mobility or serious electrical hysteresis.[10,11]

PI derivatives, which contain electron–donor (D) and electron–acceptor (A) moieties to form D–A-type co-polymers, have been successfully used in OFET-based devices.[12] A benzene ring is a chemical moiety that possesses an electron withdrawing ability to form intramolecular dipoles. In previous reports, the relationship between the conjugated length of polymer electrets and the electrical performances of organic memory transistors was constructed by bonding small molecules as side chain groups.[13,14] However, the mechanism of carrier trapping and detrapping, as well as the effects of the relationship between the electrical performances of OFETs and the spatial distribution of polar moieties in electret bulks, has yet to be clearly elucidated.

[a.] Department of Photonics, Advanced Optoelectronic Technology Centre, National Cheng Kung University, Tainan 701, Taiwan. E-mail: weiyang@mail.ncku.edu.tw; Fax: +886 6 2095040; Tel: +886 6 2757575 ext.63912
[b.] Polyimide Department, Daxin Materials Corporation, Taichung 407, Taiwan
[c.] Department of Physics, National Cheng Kung University, Tainan 701, Taiwan.
[d.] Department of Materials Science and Engineering, National Cheng Kung University, Tainan 701, Taiwan

Journal Name

ARTICLE
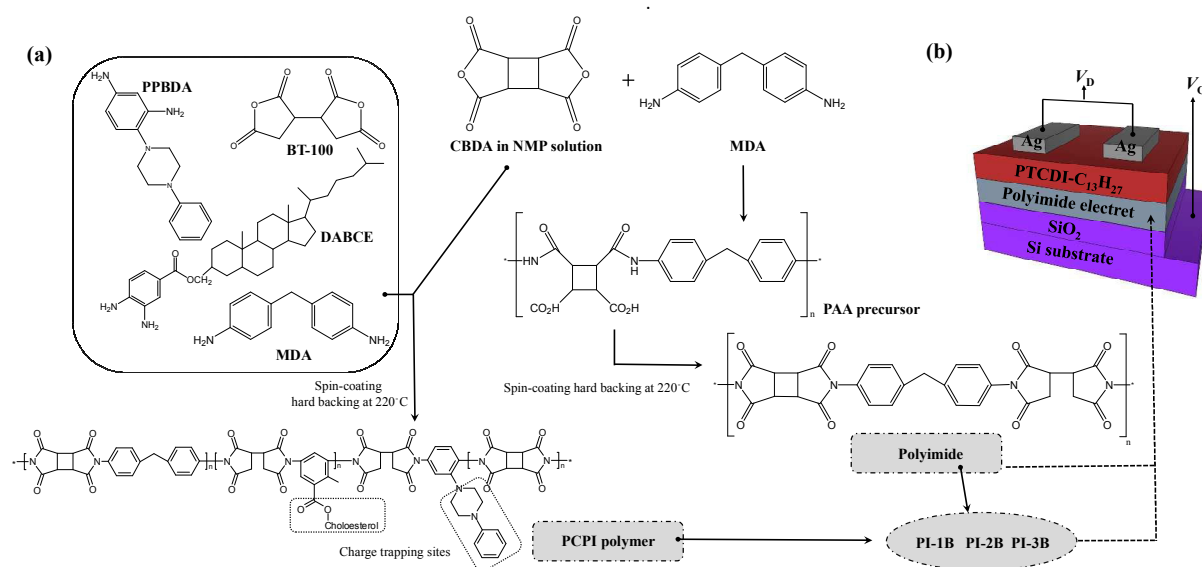
Figure1. Schematic diagram of (a) polymer additives and chemical reaction processes of polyimide electret; (b) the *n*-type organic transistor-based memory device.

In the present study, we synthesized a series of new PI electrets, which bond polar polymer molecules as side chain groups. Various ratios of the as-synthesized PI electrets were further mixed with a PI without a side chain to form a composite dielectric material that is used in OFETs and photo memory devices. The polar molecules were doped into the PI network to enhance the thermal stability of PI film; doping these molecules can extend the application of PIs in flexible electronics. We also fabricated a device with a pristine PI to serve as the control to determine the influence of the spatial distribution of the polar side chain groups within the PI films on the electrical and memory properties of the OFETs. The electrical performances of the OFETs and memories, including the on/off current ratio, field-effect mobility, and electrical hysteresis, were notably improved by increasing the ratio of the doping polar molecules. In particular, output current growth was observed in the OFETs under a long operation time. The output for the current growth of the OFETs under a long operation time could be attributed to the (a) low trap state density at the PI/organic semiconductor interface and the (b) extra carrier accumulation in the conducting channel created by the dipole-induced field. The application of these stable OFETs with our novel PIs to the field of organic memory resulted in a wide memory window by combining the photoelectric effects. In this study, we clearly elucidated the physical mechanism of the carrier trapping and detrapping of PI electrets.

2. Experimental procedures

2.1 Material Synthesis

The precursors (polyamic acid, PAA) of the PIs were prepared through the gradual addition of cyclobutane-1,2,3,4-tetracarboxylic dianhydride powder (CBDA; 23.5 g, 0.12 mmol) to n-methyl-2-pyrrolidone (NMP; 450 mL) solution. This solution was dissolved in methylenediphenyl diamine (MDA; 23.7 g, 0.12 mmol) and then stirred vigorously at room temperature for a prolonged period until it turned to a viscous/transparent solution with stable viscosity. A PI film was formed on a SiO2 substrate through spin coating and then baked at 220 °C. The piperazinyl and cholesterol groups-contained PIs (PCPIs) were prepared by poly-adding method to enhance the dipole moment of the PI polymer chains. These PCPIs were synthesized by rapidly adding antiprospective polymer 1,2,3,4-butane tetracarboxylic dianhydride powder (BT-100; 35.6 g, 0.18 mol) to the 450 mL NMP solution. The solution contained 3,5-

diamino-2-methyl-benzoic acid dihydrocholesterol ester (DABCE; 40.2 g, 0.075 mol), 4-(4-phenyl-piperazin-1-yl)-benzene-1,3-diamine (PPBDA; 20.1 g, 0.075 mol), and MDA (29.7 g, 0.15 mmol) polymers. The solution was mechanically stirred for a prolonged period until a clear viscous solution was achieved. The reaction mixture was poured into a pure toluene solution (170 mL) and then heated to 120 °C until the distillation of water stopped in a Dean-Stark apparatus to achieve a dehydration reaction. After the toluene was completely removed through distillation, 400 ml of NMP solution, which was mixed with CBDA (23.5 g, 0.12 mmol) polymer additives, was added and then stirred at room temperature until a stable viscosity was achieved. A transparent PCPI solution was obtained. Finally, various weight ratios of PCPI to PAA (6%, 10%, and 20% denoted as PI-1B, PI-2B, and PI-3B, respectively) were mixed to form PCPI films by following a similar process used in PI film fabrication. The chemical reaction processes and structures of the polymer additives are shown in Figure 1(a).

2.2 Preparation of Devices

We formed the PCPI and PI films on the n-type heavily doped silicon substrate with a 300 nm-thick SiO_2 to prepare the organic memory transistors with PI electrets. The substrate was previously cleaned with acetone, isopropanol, and deionized water for 20 min each. Afterward, oxygen plasma treatment of 30 s was performed to clean organic residues and to enhance the surface energy of SiO_2 further for the easy formations of PI and PCPI films. Then, native PI and PCPI–PI mixed polymers were spun on the silicon substrate to form a part of the gate dielectric layer and charge trapping layer of memory devices. The native PI-based memory transistor was regarded as a standard device. The n-type semiconductor N,N′-ditridecyl-1-3,4,9,10-perylenetetracarboxylicdiimide (PTCDI-$C_{13}H_{27}$) was deposited on PI films as an active layer through thermal evaporation at a rate of 0.3 Å/s. Finally, a silver film was deposited via thermal evaporation on the active layer to form source and drain electrodes. The channel width and length of the device were set to 2,000 and 100 μm, respectively, through a shadow mask. Figure 1(b) shows the structure of a PI-based organic memory transistor. All of the electrical parameters of the memory transistors were measured with a semiconductor measurement analyzer (Keithley 4200-SCS) in a nitrogen-filled glove box. The capacitance–voltage (C-V) properties and conductance measurements of all the PI-based capacitors were measured using a precision LCR meter (Agilent E4980).

3. Results and discussion

3.1 Molecular weights

The molecular weight of PIs was measured using a gel permeation chromatography (GPC) system, which was connected to a refractive index detector, at a ground temperature of 45 °C. The GPC system was calibrated with polystyrene standards; N,N-dimethylformamide served as eluent with a flow rate of 1 mL/min. The fundamental chemical properties of the synthesized PIs, such as relative number

average molecular weight (M_n), weight average molecular weight (M_w), z-average molecular weight (M_z), and protein dispersibility index (PDI), were measured using GPC.[15] Polystyrene served as a standard polymer to quantize the analyses of the molecules. The GPC results of the synthesized PIs are summarized in Table I. The PDI values of the PIs increased by increasing the mixture ratio of the PCPIs. This result indicated that the distributions of molecular weight and chain length for the PI broadened with the increase in the mixture ratio of the PCPIs. Moreover, these results confirmed that the PCPIs were effectively mixed and distributed in the PI matrix.

Table I The summarized GPC analysis of synthesized native PI and PI/PCPI mixtures in which the weight ratios of PCPI to pristine PI are 6 wt% (PI-1B), 10 wt% (PI-2B) and 20 wt% (PI-3B). M_n is number average molecular weight, M_w is weight average molecular weight, M_z is z-average molecular weight and protein dispersibility index (PDI) is defined by the ratio of M_n/M_w.

electrets	M_n	M_w	M_z	PDI
PCPI	9825	17512	28940	1.78
PI	31441	108466	187966	3.45
PI-1B	31427	109415	192723	3.48
PI-2B	24819	96129	171447	3.87
PI-3B	24862	96197	117619	3.87

3.2 Thermal properties of synthesized polymers

Differential scanning calorimetry (DSC; TA instrument TMA Q400EM) was conducted to analyze the thermal properties of the PIs. The physical consuetude, such as phase transition and the spatial distribution of PCPI polymers in the polymer backbone of PIs, could be explained via this measurement. The solid-type PI films were scraped down from the substrate and then sealed with a metal griddle. Subsequently, the griddle was placed into the instrument to measure the heat capacity of the PIs. The sample was heated to 50 °C and held for 5 min prior to DSC temperature scanning. The scan was performed from 50 °C to 300 °C with a heating rate of 20 °C/min. The T_g values of the PIs were obtained from the peak of the differential relationship between the heat flux and the temperature in the thermal transfer curves. Figure 2 shows a glass transition process and a curve of heat flux versus temperature; this process involved slow heating below the glass transition temperature, T_g. To accurately obtain the T_g, the derivative of the heat flux with respect to temperature were performed on the temperature-dependent DSC curves of all PIs (see Figure S1). Two different conventions, namely, exothermic and endothermic reactions in the PIs, showed a negative peak in these curves at approximately 240 °C; this result is consistent with those of previous reports for PIs.[16,17]

ARTICLE
Journal Name
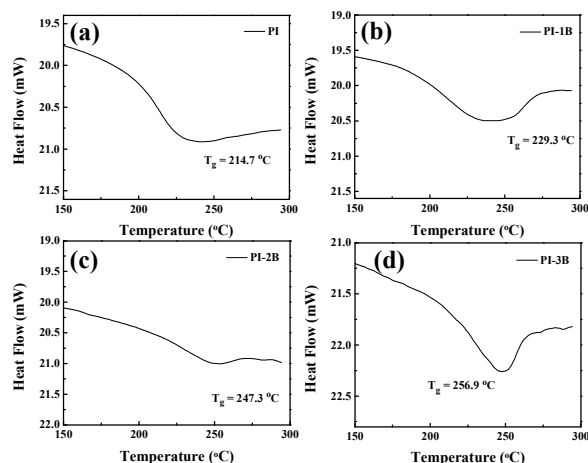
Figure 2. The temperature-dependent DSC curves of native PI and PCPI mixed polymers with different weight ratios of PCPIs: (a) 0, (b) 6%, (c) 10%, and (d) 20%.

As the PCPI was doped into the PI, the T_g became notably large. Moreover, T_g increased with the increase in the amount of doping PCPI. This phenomenon could be attributed to the interaction of the polymer chains being enhanced by the introduction of polar side chains. The DSC results also confirmed that the PCPI effectively mixed with the PI at the side chain position. Thus, the highest T_g value for the PI-3B film revealed that the highest densities of piperazinyl and cholesterol side chains were contained within the PI in the polymer matrix. Heat energy had to be consumed to overcome the intermolecular interaction force during the phase transition because of the enhancement of the intermolecular interaction of the neighboring molecules by the polar side chain. The large T_g of the PI film resulted in a high amount of PCPI polymers distributed in the PI solid films.
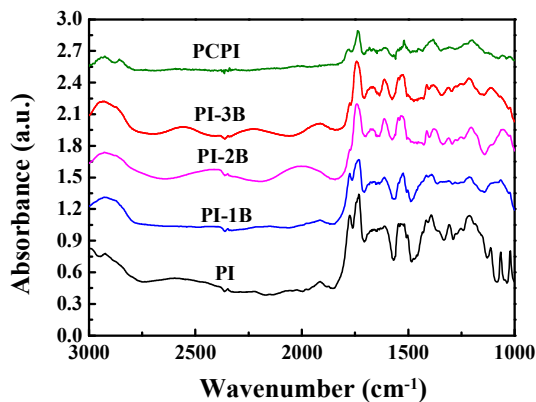
Figure 3. The FTIR spectra of synthesized PI dielectrics PI, PCPI, PI-1B, PI-2B, and PI-3B in absorption mode at a resolution of 4 cm^{-1}. The feature of spectrum is averaged for scanning 32 times and the wave numbers of measurement range from 3300 cm^{-1} to 900 cm^{-1}.

Accordingly, T_g was positively correlated with the density of the PCPIs within the polymer matrix. This finding indicated the existence of quasi-permanent polarization fields in the piperazinyl and cholesterol groups. The enhancement of T_g via PCPI polymer doping would benefit PI applications in flexible substrates.

3.3 Structural analysis

The synthesized PIs were resolved via Fourier transform infrared spectroscopy (FTIR; Varian 660-IR) under absorption mode to realize their chemical structure. The measured sample was prepared using a spin coating method to form thick solid PI films on the cleaned silicon wafer. Then, the sample was scanned from 500 cm^{-1} to 2500 cm^{-1} wavenumbers under a nitrogen-filled environment. The FTIR spectra of the PI polymers were expressed by the average data of 32 scans. The characteristic absorption bands, which were related to the chemical bonds of the PI films, are shown in Figure 3. The peaks located at 1,745 and 1,774 cm^{-1} corresponded to the typically unsymmetrical and symmetrical C=O stretching of PIs, respectively.[18] A recognizable 1,774 cm^{-1} peak can be observed in the PI and PI-1B films, but the same cannot be obviously observed in the films of PI-2B and PI-3B. This phenomenon might be attributed to the degree of spatial freedom for symmetrical C=O stretching that was restricted by a high density of piperazinyl and cholesterol groups within the PI film.

The characteristic absorption bands at around 1,523 and 1,200 cm^{-1} were clearly observed in the FTIR spectra for all the PIs; these bands corresponded to the typical vibrations of imide rings.[18,19] Notably, the absorption peaks at 1,612 and 1,660 cm^{-1}, which correspond to cyclopentene vibration and the C=O stretching of benzaldehyde compound[20], respectively, for PI-B electrets are stronger than those in the PI. This phenomenon might be attributed to numerous benzaldehyde compounds.

A relatively broad absorption peak at 2,929 cm^{-1} related to the stretching vibration of C-H bonds of methyl compounds with a cholesterol structure was observed in the PI-B electrets.[21] The above result confirmed that the PCPI groups with intrinsic polarity were successfully bonded on the PI backbone to form PCPI electrets. Strong electrical dipoles could be induced under an external electric field to provide charge trapping sites for the application in memory devices because of the quasi-permanent dipoles on the PI-B side chains.
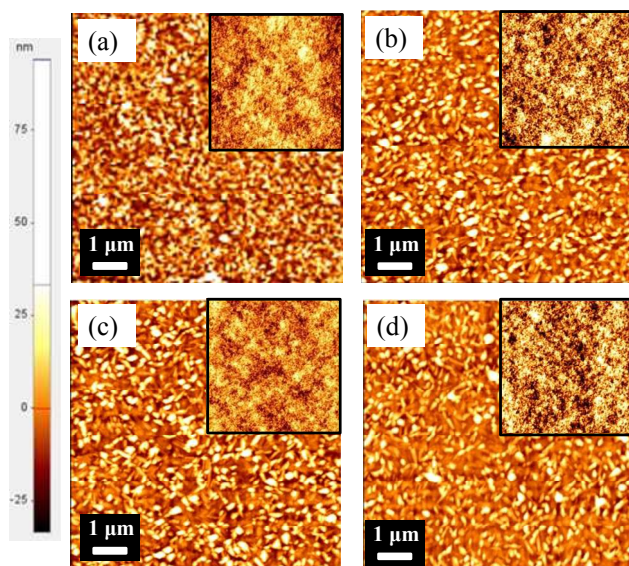
Figure 4. AFM images of PTCDI films growth on different gate electrets: (a) native PI, (b) PI-1B, (c) PI-2B, and (d) PI-3B. All images are 10 μm × 10 μm in size. (Inset: pristine features of PI electrets on the top of oxygen plasma-treated SiO_2 surface.)

Table II The summarized surface properties of synthesized native PI and PCPI films in which the weight ratios of PCPI to pristine PI are 6% (PI-1B), 10% (PI-2B), and 20% (PI-3B). The surface roughnesses of following deposited PTCDI-$C_{13}H_{27}$ films are also included.

[a] The root mean square roughness of films.

films	PI	PI-1B	PI-2B	PI-3B
R_q (nm)[a]	0.18	0.24	0.27	0.25
R_q (nm) (with PTCDI)	9.95	9.90	10.80	11.10

3.4 Surface morphology properties

The surface properties of dielectric layers affect the electrical performance of field-effect transistors.[22–25] In our work, we used an atomic force microscope (AFM; Park system XE-100) to obtain the surface properties of the PI dielectrics that were deposited on a silicon substrate. The insets of Figure 4 show that the surface morphologies of the pristine PI and PI-B films were extremely smooth without any structural defects and fluctuation. Table II reveals that the surface of the PI-B films is slightly rougher than that of the PI films. The as-deposited PTCDI-$C_{13}H_{27}$ films exhibit strip-style grains on the PI films. This observation demonstrated the high degree of crystalline PTCDI-$C_{13}H_{27}$ film. Table II shows that the surface roughness of the PTCDI-$C_{13}H_{27}$ films increases by increasing the PCPI ratio. This result could be attributed to the increase in polarity on the PI surface by increasing the number of polar side chains. This increase in polarity led to the 3D growth of the PTCDI-$C_{13}H_{27}$ molecules. Although the roughness of the

PTCDI-$C_{13}H_{27}$ films depended on the number of polar side chains within the PI, the crystal structure, including the crystalline size and disorder of these semiconductor films obtained from the analyses of Figure 5, was nearly the same.

3.5 Electrostatic force microscopy imaging

The distribution of electric field gradients on gate dielectric surfaces significantly affects the electrical performances of OFETs. Electrostatic force microscopy (EFM) the tip scanning technique is a reliable tool to analyze the surface potential and bulk conductivity of materials.[26] A given sample bias-induced field gradient on a dielectric surface can cause phase variance in an EFM image.[27,28] Therefore, the gradient of a dipole-induced electric field generated by PCPI side chains on a PI surface can be evaluated through the phase variation of an EFM image. The EFM phase diagrams of the PI films in this study are demonstrated in Figure 6, which shows that the level of phase variance increased with the increase in the ratio of the PCPI polymer. Figure 6(e) shows the statistical phase variances of the PI films with different densities of PCPI polymers. The phase variation increased with the increase in the ratios of the PCPI polymers, thus indicating that the polar side chains induced a field gradient on the PI surface. A large dipole-induced field is expected to accumulate numerous carriers in the conducting channel of OFETs and to trap numerous carriers on the organic semiconductor/electret surface for OFET-based memory during programming.
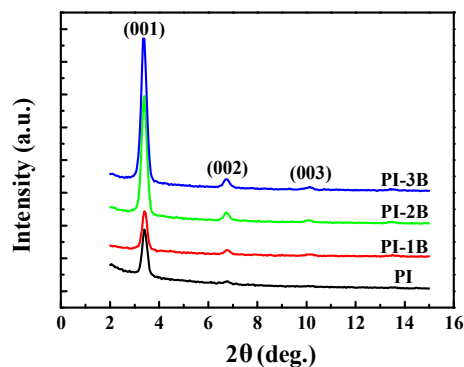
Figure 5. *X*-ray diffraction spectra of PTCDI-$C_{13}H_{27}$ films grown on native PI, PI-1B, PI-2B, and PI-3B films. The thicknesses of all PTCDI-$C_{13}H_{27}$ films are 60 nm.
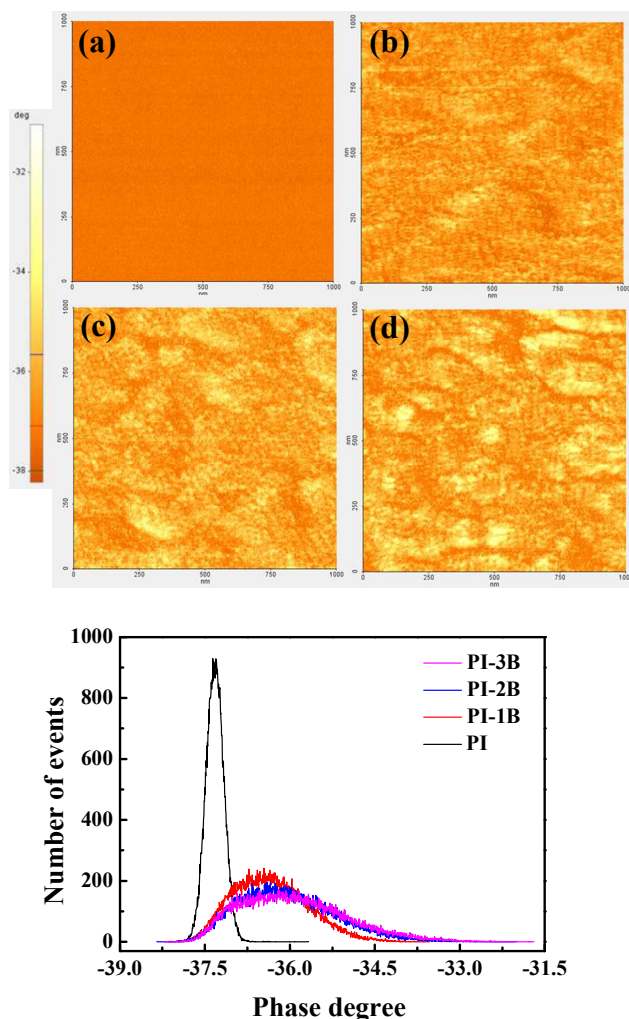
Figure 6. The phase variances of (a) native PI, (b) PI-1B, (c) PI-2B, and (d) P1-3B films on cleaned indium tin oxide (ITO) glass substrates on which the same bias of +1 V is applied on ITO electrodes. Scanning EFM images are 1 μm × 1 μm in size. (e) Statistical data of phase distribution is obtained from above EFM images.

3.6 Electrical properties

Figure 7 shows the output characteristics of organic memory transistors with PI electrets as both gate dielectric and charge storage layers. The saturation drain current evidently decreased with the reduction in the number of polar side chain groups. This finding indicates that the charge accumulation capacity at the interface of a semiconductor and a PI layer can be enhanced by increasing the spatial intensity of side chain groups, which are bonded to the backbone of PI molecules. However, the organic memory transistor with pure PCPI electret has the smallest saturation drain current (see Figure S2) because the high surface energy of the PCPI film results in a bad crystal quality of following PTCDI-$C_{13}H_{27}$ deposition and high gate leakage current occurs in pure PCPI-based OFET. Accordingly, the pure PCPI cannot be used alone as electret in the fabrication of OFET.
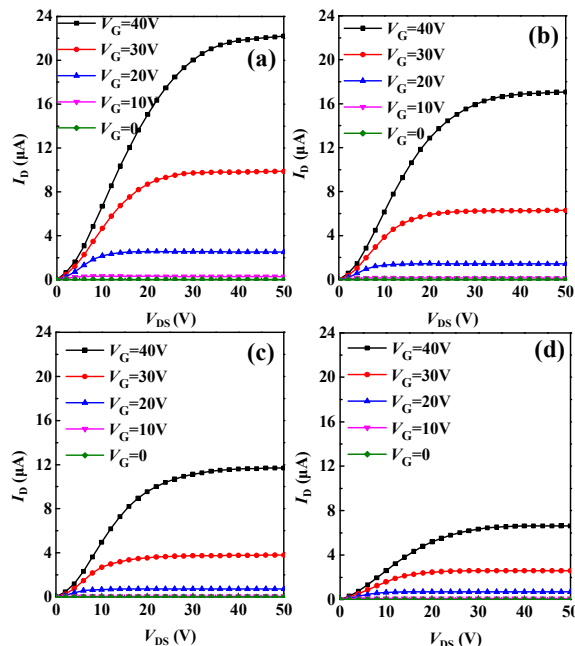
Figure 7. The output characteristics of n-type OFET-based memory devices that embedded with (a) PI-3B, (b) PI-2B, (C) PI-1B, and (d) native PI polymers between semiconductor and SiO_2 layer.

Table III The summarized electrical characteristics of OFET-based memory devices with native PI, PCPI, PI-1B, PI-2B, and PI-3B polymers as gate electrets.

Dielectrics	V_t (V)	μ (cm^2/Vs)	on/off ratio	SS (V/decade)	C_{ox} (nF/cm^2)
PI	13.35	0.13	1.43×10^5	2.68	8.47
PCPI	21.20	0.16	9.93×10^3	3.18	8.87
PI-1B	22.07	0.30	1.05×10^5	2.51	8.99
PI-2B	21.12	0.38	1.29×10^5	2.90	9.61
PI-3B	19.22	0.41	1.2×10^5	3.74	10.06

These unspecified carbon groups, such as alkyl, benzene ring, and alkene, can form quasi-permanent dipoles because of the polarization of delocalized π-electrons under an external electric field. These dipoles can aid in the additional accumulation of charge carriers localized in the conducting channel of a semiconductor layer when a negative bias is applied to the gate electrode of OFETs. Hence, the saturation current of the device may be increased when PCPI with a high doping ratio is used. For comparison, Figure 7(d) shows the output characteristics of an organic memory transistor with a PI (no polar side chains) as a charge-trapping layer and reveals the lowest saturation currents in all memory transistors. This result indicates that PCPIs are a critical element to achieve high-performance organic memory transistors.

The electrical parameters of the OFETs with different electrets are presented in Table III. The field-effect carrier mobility (μ) of an

OFET can be calculated using the drain current-related formula of ID with respect to gate bias V_G:[29]

$$I_{D_{SAT}} = \frac{W\mu C_i}{2L}(V_G - V_t)^2 , \qquad (1)$$

where L and W are the channel length and width, respectively, C_i is the capacitance per unit area of the gate dielectric, and V_t is the threshold voltage. The subthreshold swing SS of the OFET is defined as follows:

$$SS = \left[\frac{\partial\left(\log I_D\right)}{\partial V_G} \right]^{-1} . \qquad (2)$$

The capacitances of PI electrets are enhanced by doping PCPI molecules because of the induction of polarization in the polar groups under an external electrical field. This accumulation of polarization-enhanced charges in the conducting channel of OFETs leads to the increase of the μ of memory devices with PI-B series electrets in comparison with the native PI-based memory device with an electron mobility value that is greater than the reported research values for *n*-type OFETs.[30–32] We measured the frequency-dependent capacitance on the PI dielectrics with metal–insulator–metal MIM structure to elucidate further the charge transport mechanism near the PI/semiconductor interface.

Figure 8 shows the frequency-dependent capacitance of the PI-based capacitors. The capacitances of all the samples notably increased at the low frequency region (the detailed features of the frequency-dependent capacitances are displayed in the inset) and became saturated to a similar value at the high frequency region. The capacitance and frequency response of the PI-B series dielectrics increased with the increase in the doping amount of PCPI molecules, which benefits the enhancement of carrier mobility and operating speed of OFETs.[33]
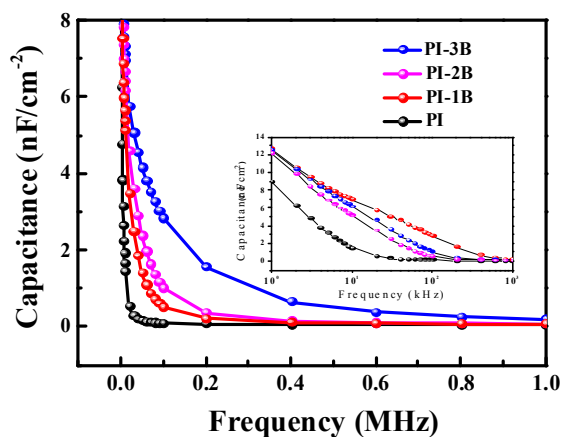
Meanwhile, the capacitance of native PI-based capacitor is relatively lower than that of PCPI-doped dielectrics. The measurements of capacitance directly prove that the dipole field induced by PCPI molecules in a PI network can effectively accumulate carriers in capacitors and OFET-conducting channels. Therefore, in this work, the number of charged carriers that accumulated at the PI/organic semiconductor interface was closely related to the spatial density of the PCPI molecules.

The electrical stability of organic devices is an important issue that must be addressed when applying large integrated circuits, except for those with superior electrical performances. The electrical hysteresis of transistors, which is caused by the charge trapping behavior, is the main cause of the electrical instability of transistors. Given the charge trapping states generated by residual ions in dielectrics, the crystalline boundaries of polymer crystals, or the lattice mismatch among heterogeneous junctions, the activity of carrier transportation is limited by these states. These carriers restricted by trapped states may deplete the charged carrier density and may shield the effective electric field conducted by the semiconductor layer, thereby resulting in the electrical instability of transistors for long operation periods.

The saturation output currents of transistors generally decrease with an increase in operation time because of the charge trapping effect at the interface between the dielectric and active layers.[34–36] Over the past decade, numerous studies have proposed that the output currents of SiO_2-based organic transistors drop after continuous and repeated operations because of the deep-trap states contributed by silanol groups on the SiO_2 surface.[37,38] Figure 9 shows the time-dependent drain current characteristics of PI- and PCPI-based memory transistors under a high electrical bias stress (V_G = 40 V). The time-dependent electrical behavior of our devices is contrary to those of previous reports, that is, no current decay occurred under a long operation time of 10^4 s. This result indicates that OFETs with PI or PCPI dielectrics are stable organic devices. We can speculate that with the high electrical stability of memory transistors with PI or PCPI dielectrics, the charged carriers are compensated in the conductive channel.[39] In this work, near quasi-permanent dipoles were formed on the piperazinyl and cholesterol side chain moieties of the PCPIs when a positive bias was constantly applied on the gate electrode. These transient dipoles can attract extra electrons on the dielectric/semiconductor interface to fill up the defects within the conductive channel that are generated by the gate bias stress.

Figure 8. The frequency-dependent capacitance properties of PI electret-based capacitors; the applied voltage between two electrodes is 40 V.
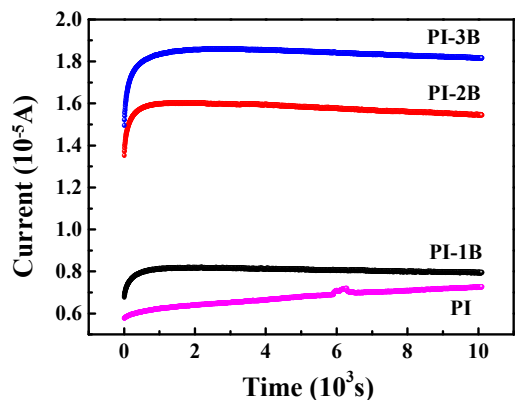
Figure 9. The time-dependent output drain currents of the OFET-based memory devices with different polymeric gate electrets under constant bias: V_D and V_G are 50 V and 40 V, respectively.
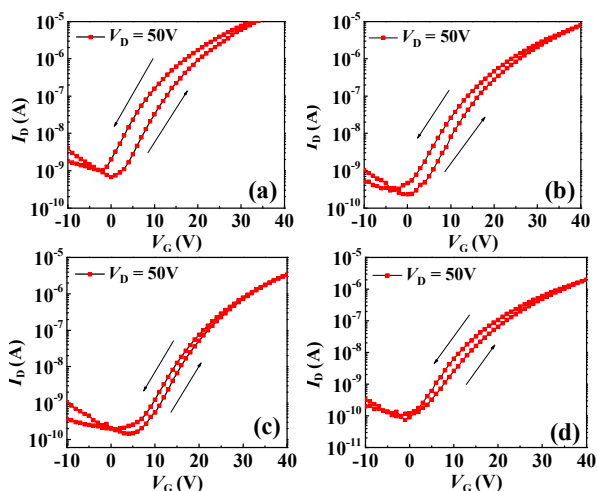
Figure 10. Hysteresis characteristics of the OFET-based memory devices with (a) PI-3B, (b) PI-2B, (C) PI-1B, and (d) native PI polymer gate electrets. The V_D keeps at 50 V and V_G scans from -10 V to 60 V.

The feature of the charge compensation phenomenon in the conductive channel was indirectly verified by the time-dependent transfer characteristics of the PI- and PCPI-based transistors, as shown in Figure 9. A current growth phenomenon was observed in the time-dependent electrical measurements for all the organic transistors at the initial state. This phenomenon of current growth can be attributed to the amount of dipole field-assisted carrier accumulations beyond the consumed charge carriers in the conductive channel by the gate bias-induced trap states. The time-dependent drain current of the memory transistors with the native PI dielectrics exhibited a persistently increasing phenomenon under a long operation time of 10^4 s. This increasing phenomenon was caused by a weak dipole, which was gradually polarized within the polymer chain of the native PI. Accordingly, the slow polarization effect on the polar moiety of PCPI molecules can overcome the stability issue of organic transistors, thereby leading to organic devices with high stability for future applications.

3.7 Charge transport properties

The interfacial carrier transportation properties at the PI/semiconductor layer were attained with the electrical hysteresis behavior of memory devices. This hysteresis behavior was obtained by measuring the I_D versus V_G curves of the OFET transistors under forward and backward sweeping of V_G within the range of −10 and 40 V. In previous reports, the proportion of hysteresis areas obtained from sweeping the I_D-V_G curves was strongly dependent on the density of the trap states at the active/dielectric interface.[40–42] Figure 10 shows the hysteresis curves of the memory devices with PI electrets that possess different densities of PCPI molecules. A low hysteresis level is presented in Figure 10 for all the PI- and PCPI-based devices. The result indicates that our PI polymer dielectrics can achieve a near trap-free surface at the active/PI interface. The polar functional groups of polymer dielectrics are generally considered the origin of interfacial defects, supplying the carrier trapping states at interfaces and electrically unstable output currents of OFETs.[33,39] However, Figure 10 reveals that our memory devices underwent minimal electrical hysteresis under the rapid switching of voltage scans. This finding was attributed to the rapid orientation of the electrical dipoles on the PCPI side chain moiety by applying a gate field. We speculated that the rapid transferable dipole direction could be quickly oriented and reoriented during sweeping voltage scans. Hence, a high frequency response for organic devices, such as memories and photosensors, can be expected.

3.8 Organic memory devices

Organic material-based optoelectronics, in which electrical devices combine with photo-induced effects, have a great potential in optical-driving logic circuits. Over the past two decades, high-performance organic optoelectronics, such as phototransistors, photo memories, and photosensors, have been fabricated.[43,44]

Photo-induced effects can effectively enlarge the electrical memory windows of organic memories to avoid unrecognized storage data. Figure 11 shows the transfer characteristics of memory transistors with different PI electrets upon the application of a programming voltage pulse of 90 V/1 s, erasing voltage pulse of −90 V/5 s, and erasing voltage pulse of −90 V/5 s combined with the green light pulse of 532 mm wavelength. Programming and erasing operations are conducted on memory devices; thus, the memory window is defined as the threshold voltage difference between these two operations. Programming carriers cannot be erased easily through the erasing operation without light pulse assistance for all memories because they are strongly trapped within the polar groups of PCPIs.
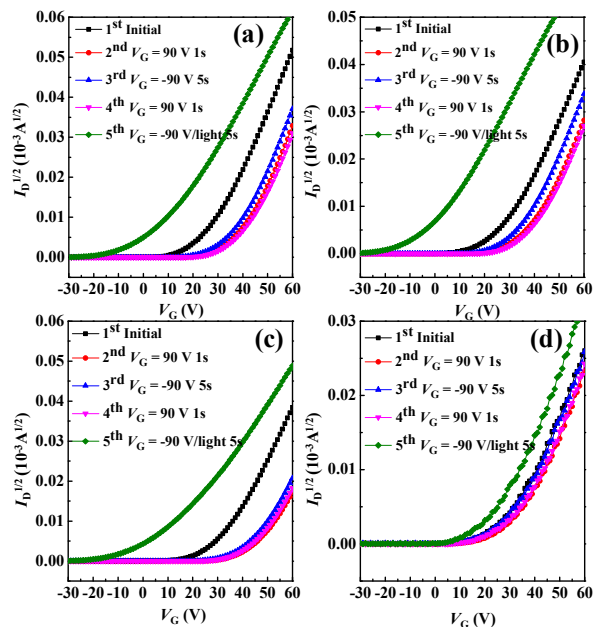
Figure 11. Transfer properties of the OFET-based memory devices with (a) PI-3B, (b) PI-2B, (C) PI-1B, and (d) native PI polymer gate electrets as charge trapping layer. A positive voltage of 90V is applied on the gate during programming process, and a -90 V gate voltage and light irradiation with wavelength of 532 nm as well as intensity of 15.8 mW/cm^2 are applied on the devices during erasing process.

Few carriers can be programmed into the memory device with native PI electret (no polar side chains), as shown in Figure 11(d). In this work, the memory windows of all the devices, except for the device with a native PI electret, were remarkably enhanced when the irradiation-assisted erasing operation was performed on all the memory devices. All of the values of the memory windows of the devices with various ratios of PCPI-doped PI electrets are shown in Table IV. The function of irradiation assistance in the erasing process is to create a minority of PTCDI-C$_{13}$H$_{27}$, that is, holes that recombine the trapped electrons induced by the programming pulse to result in a large negative shift of V_t. When light irradiates the channel region of a memory device during the erasing operation, photo-generated hole-electron pairs are created and then dissociated by the gate field to form mobile carriers.[45] The memory window slightly decreases with an increase in the spatial density of PCPI molecules because more electrons are trapped by higher ratio of PCPI molecules. Accordingly, PCPI polymer is potentially used in the electret of organic memory devices.
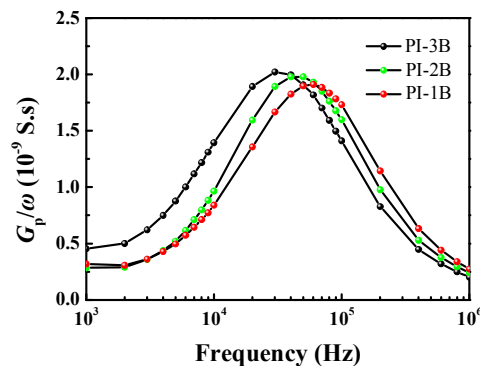
Figure 12. The curves of G_p/ω versus signal frequency for PI-based MISM diodes in inversion region; the applied voltage between parallel electrodes is 5 V.

Table IV The threshold voltage obtained from fresh devices and after programming and erasing processes. Large electrical memory windows are achieved by using irradiation-assistant erasing operations.

Dielectrics	Initial (V)	Writing 1s (V)	Erasing 5s (V)	Memory window (V)
PI - 3B	25.8	39.4	6.4	33.0
PI - 2B	27.1	37.5	1.4	36.1
PI - 1B	30.1	43.8	5.6	38.2

The interface trap state density (D_{it}) and interface trap constant time (τ_{it}) at the PI/semiconductor interface should be understood to elucidate the role of the memory windows of devices with PI electrets in the issue of the spatial density of PCPIs. The conductance method is reliable in quantifying these physical quantities among PI/semiconductor interfaces.[46,47] These two interface-related physical quantities can be obtained from the measurements of equivalent parallel capacitance and parallel conductance (G_p) of a metal–insulator–semiconductor–metal (MISM) capacitor. G_p is defined as follows:

$$\frac{G_P}{\omega} = \frac{q\omega\tau_{it}D_{it}}{1+(\omega\tau_{it})^2},$$ (3)

where q is the electron charge and ω is the angular frequency of measurement. Figure 12 shows the typical behavior of frequency-dependent conductance curves for PI-based MISM capacitors. The τ_{it} of the interface states is obtained with the formula $\omega\tau_{it} = 1$ at the maximum of curves. The D_{it} values of the MISM diodes with different PI electrets are calculated using Equation (3). The D_{it} at the dielectric/semiconductor interface is one of the key issues affecting the electrical stability of OFETs under a long operation time. The calculated Dit at the interface of PI/PTCDI-C$_{13}$H$_{27}$ lies between 2.4 $\times$ 10^{10} and 2.7 $\times$ 10^{10} eV^{-1} cm^{-2}; this value is considerably lower than that of the interface of SiO$_2$/organic semiconductor in previous

reports.[48,49] Such low interface state density leads to low electrical hysteresis and high electrical stability for memory transistors with PI electrets. Despite the low interface trap sites at the interface, a large amount of electrical memory window can still be obtained. In this study, we proposed that the injection carriers were trapped into/released from the shallow trap states, that is, low τ_{it} (Table V), thereby forming in the PCPI side chain groups during the programming/erasing operations. τ_{it} increases with an increase in the ratio of PCPI molecules within PI polymers. Therefore, trapped carriers cannot be removed easily from memory devices with a high ratio of PCPI molecules during the erasing process. This condition results in the reduction of memory windows. In sum, we achieved memory transistors with high stability and superior memory properties using PI/PCPI composited electrets with low D_{it} and short τ_{it} at the PI/semiconductor interface.

Table V The calculated interface trap state density (D_{it}) and the interface trap constant time (τ_{it}) of metal-insulator-semiconductor-metal (MISM) capacitor at PI/semiconductor interface.

Dielectrics	D_{it} (10^{10} eV^{-1} cm^{-2})	τ_{it} (μs)
PI-3B	2.53	5.31
PI-2B	2.48	3.98
PI-1B	2.65	2.65

4. Conclusions

We successfully synthesized new PI electrets with dual-charge (electron and hole) withdrawing ability. This synthesis was achieved by bonding polar piperazinyl and cholesterol side chains on the PI backbone, the chemical structure of which was verified through FTIR analyses. PIs serve as charge-trapping elements and gate dielectrics for memory devices based on electron-dominating OFETs. The GPC results show that the PDI values of the PI- and PCPI-mixed solutions slightly increased with the increase in the weight ratio of the PCPI molecules. This increase was caused by the expansion of the spatial distribution of the PCPIs in the electret matrix. The enhanced thermal properties of PI electrets resulting from the increased doping ratios of PCPI molecules would benefit the application of PIs in flexible electronics. When the PI films were formed on the SiO$_2$ substrates, the ultrasmooth surfaces of the PI electrets in this work led to the formation of well-ordered PTCDI-C$_{13}$H$_{27}$ crystals on the PI films. The introduction of polar side chains into the PI network resulted in the accumulation of extra carriers within the conducting channel of the organic transistors via the polar group-induced dipole field and in the attraction of electrons to the dipole field for the n-type organic memory. Such polarization effect was demonstrated through the EFM and capacitance analyses. The electrical characteristics of the organic transistors with PI dielectrics, such as the field-effect carrier mobility, output current, and on/off current ratio, were enhanced by increasing the weight ratio of the PCPI molecules. The most significant breakthrough for the OFETs with PIs as dielectrics was the output current growth under a long operation time, which could improve the poor stability of organic transistors. An excellent memory window of more than 38 V was achieved for the photo-assisted organic memory with PI as an electret; here, the injection electrons were trapped into the dipole field and were erased by irradiation-induced holes. Accordingly, our novel PI with polar side chains improves the stability of OFETs and enlarges the organic memory. This novel PI also has the potential to be applied to other flexible electrical devices, such as multifunctional organic photoelectric devices, biosensors, and flexible substrates.

Notes and references

1   Y. Diao, B. C.-K. Tee, G. Giri, J. Xu, D. H. Kim, H. A. Becerril, R. M. Stoltenberg, T. H. Lee, G.Xue, S. C. B. Mannsfeld, Z.Bao, *Nature Mater.* ,2013, **12**, 665-671.

2   H. Yan, Z. Chen, Y. Zheng, C. Newman, J. R. Quinn, F. Dotz, M. Kastler, A. Facchetti, *Nature*, 2009, **457**, 679–687.

3   P. Heremans, G. H. Gelinck, R. Muller, K. J. Baeg, D. Y. Kim, Y. Y. Noh, *Chem. Mater.*, 2011, **23**, 341-358.

4   M. Egginger, M. I. Vladu, R. Schwödiauer, A. Tanda, I. Frischauf, S.Bauer, N. S. Sariciftci, *Adv. Mater.*, 2008, **20**, 1018-1022.

5   Q. D. Ling, D. J. Liaw, E. Y. H. Teo, C. Zhu, D. S. H. Chan, E. T. Kang, K. G. Neoh, *Polymer*, 2007, **48**, 5182-5201.

6   Q. D. Ling , F. C. Chang , Y. Song, C. X. Zhu, D. J. Liaw, D. S. H. Chan, E. T. Kang, K. G. Neoh, *J. Am. Chem. Soc.*, 2006, **128**, 8732-8733.

7   Y. Guo, C. Di, S. Ye, X. Sun, J. Zheng, Y. Wen, W. Wu, G. Yu, Y. Liu, *Adv. Mater.*, 2009, **21**, 1954-1959.

8   K. J. Baeg, Y. Y. Noh, J. Ghim, S. J. Kang, H. Lee, D. Y. Kim, *Adv. Mater.*, 2006, **18**, 3179-3183.

9   K. J. Baeg, Y. Y. Noh, J. Ghim, B. Lim, D. Y. Kim, *Adv. Funct. Mater.*, 2008, **18**, 3678-3685.

10 R. Ahmed, C. Simbrunner, G. Schwabegger, M.A. Baig, H. Sitter, *Org. Electron.*, 2014, **15**, 3203-3210.

11 K. J. Baeg, A. Facchettic, Y. Y. Noh, *J. Mater. Chem.*, 2012, **22**, 21138.

12 Y. H. Chou, N. H. You, T. Kurosawa, W. Y. Lee, T. Higashihara, M. Ueda, W. C. Chen, *Macromolecules*, 2012, **45**, 6946-6956.

13 Y. H. Chou, Y. C. Chiu, W. Y. Lee, W. C. Chen, *Chem. Commun.*, 2015, **51**, 2562.

14 K. Takagi, T. Nagase, T. Kobayashi, H. Naito, *Org. Electron.*, 2014, **15**, 372-377.

15 H. He, M. Zhong, B. Adzima, D. Luebke, H. Nulwala, K. Matyjaszewski, *J. Am. Chem. Soc.*, 2013, **135**, 4227-4230.

16 D. J. Liaw, P. N. Hsu, W. Hs. Chen, S. L. Lin, Macromolecules, 2002, **35**, 4669-4676.

17 M. A. Meador, *Annu. Rev. Mater. Sci.*, 1998, **28**, 599-630.

18 Y. Chen, J. O. Iroh, *Chem. Mater.*, 1999, **11**, 1218-1222.

ARTICLE

19 J. C. Huang, C. B. Hea, Y. Xiao, K. Y. Mya, J. Dai, Y. P. Siow, *Polymer*, **44**, 2003, 4491-4499.

20 T. L. Li, S. L. C. Hsu, *European Polymer Journal*, 2007, **43**, 3368-3373.

21 M. M Paradkar, J. Irudayaraj, *International Journal of Dairy Technology*, 2002, **55**, 127-132.

22 Y. H. Yang, S. H. Kim, L. Yang, S. Y. Yang, C. E. Park, *Adv. Mater.*, 2007, **19**, 2868-2872.

23 K. Shin, S. Y. Yang, C. Yang, H. Jeon, C. E. Park, *Org. Electron.*, 2007, **8**, 336-342.

24 Y. Jung, R. J. Kline, D. A. Fischer, E. K. Lin, M. Heeney, I. McCulloch, D. M. DeLongchamp, *Adv. Funct. Mater.*, 2008, **18**, 742-750.

25 S. Kobayashi, T. Nishikawa, T. Takenobu, S. Mori, T. Shimoda, T. Mitani, H. Shimotani, N. Yoshimoto, S. Ogawa, Y. Iwasa, *Nature Mater.*, 2004, **3**, 317.

26 P. Girard, *Nanotechnology*, 2001,**12**, 485.

27 H. N. Raval, D. S. Sutar, P. R. Nair, V. R. Rao, *Org. Electron.*, 2013, **14**, 1467.

28 H. N. Raval, D. S. Sutar, V. R. Rao, *Org. Electron.*, 2013,**14**, 1281.

29 J. Zaumseil, H. Sirringhaus, *Chem. Rev.*, 2007, **107**, 1296-1323.

30 U. Zschieschang , K. Amsharov , M. Jansen , K. Kern, H. Klauk, R. T. Weitz, *Org. Electron.*, 2015, **26**, 340-344.

31 E. J. Puigdollers, M. D. Pirriera, A. Marsal, A. Orpella, S. Cheylan, C. Voz , R. Alcubilla, *Thin Solid Films*, 2009, **517**, 6271-6274.

32 E. B. Cho, S. H. Yu, M. Kim, M. H. Lee, W. Huh, J. Lee, J. Kim, J. H. Cho, J. Y. Lee, Y. J. Song, M. S. Kang, *J. Phys. Chem. C*, 2014, **118**, 18146-18152.

33 E. M. Aghamohammadi, R. Rödel, U. Zschieschang, C. Ocal, H. Boschker, R. T. Weitz, E. Barrena, H. Klauk, *ACS Appl. Mater. Interfaces*, 2015, **7**, 22775-22785.

34 T. Miyadera, S. D. Wang, T. Minari, K. Tsukagoshi, Y. Aoyagi, *Appl. Phys. Lett.*, 2008, **93**, 033304.

35 D. K. Hwang, C. F. Hernandez, M. Fenoll, M. Yun, J. Park, J. W. Shim, K. A. Knauer, A. Dindar, H. Kim, Y. Kim, Jungbae Kim,H. Cheun, M. M. Payne, S. Graham, S. Im, J. E. Anthony, B. Kippelen, *ACS Appl. Mater. Interfaces.*, 2014, **6**, 3378-3386.

36 U. Zschieschang, K. Amsharov, M. Jansen, K. Kern, H. Klauk, R. T. Weitz, *Org. Electron.*, 2015, **26**, 340-344.

37 L. L. Chua, J. Zaumseil, J. F. Chang, E. C. W. Ou, P. K. H. Ho, H. Sirringhaus, R. H. Friend, *Nature*, 2005, **434**, 194-199.

38 R. P. Ortiz, A.Facchetti, T. J. Marks, *Chem. Rev.*, 2010, **110**, 205-239.

39 H. L. Cheng, J. W. Lin, J. Ruan, C. H. Lin, F. C. Wu, W. Y. Chou, C. H. Chen, C. K. Chang, H. S. Sheu, *ACS Appl. Mater. Interfaces*, 2015, **7**, 16486-16494.

40 B. Lee, A. Wan, D. Mastrogiovanni, J. E. Anthony, E. Garfunkel, V. Podzorov, *Phys. Rev. B*, 2010, **82**, 085302.

41 E. Orgiu, S. Locci, B. Fraboni, E. Scavetta, P. Lugli, A. Bonfiglio, *Org. Electron.*, 2011, **12**, 477-485.

42 C. Liu, Y. Xu, Y. Li, W. Scheideler, T. Minari, *J. Phys. Chem. C*, 2013, **117**, 12337-12345.

43 S. Dutta, K. S. Narayan, *Adv. Mater.*, 2004, **16**, 2151-2155.

44 Y. Liu, Q. Shi, L. Ma, H. Dong, J. Tan, W. Hua, X. Zhan, *J. Mater. Chem. C*, 2014, **2**, 9505.

45 W. L. Leong, N. Mathews, S. Mhaisalkar, Y. M. Lam, T. Chenb, P. S. Lee, *J. Mater. Chem.*, 2009, **19**, 7354-7361.

46 K. Martens, C. O. Chui, G. Brammertz, B. D. Jaeger, D. Kuzum, M. Meuris, M. M. Heyns, T. Krishnamohan, K. Saraswat, H. E. Maes and G. Groeseneken, *IEEE Trans. Electron Devices*, 2008, **55**, 547-556.

47 R. E. Herbert, Y. Hwang, S. Stemmer, *J. Appl. Phys.*, 2010, **108**, 124101.

48 S. Lee, S. J. Kang, G. Jo, M. Choe, W. Park, J. Yoon, T. Kwon, Y. H. Kahng, D. Y. Kim, B. H. Lee, T. Lee, *Appl. Phys. Lett.*, 2011, **99**, 083306.

49 D. M. Taylor, J. A. Drysdale, I. Torres, O. Fernández, *Appl. Phys. Lett.*, 2006, **89**, 183512.

RSC Advances Accepted Manuscript

ARTICLE

Table of Contents

Controlling carriers trapping and relaxation with a dipole field in an organic field-effect device

Yu-Fu Wang, Min-Ruei Tsai, Po-Yang Wang, Chin-Yang Lin, Horng-Long Cheng, Fu-Ching Tang, Steve Lien-Chung Hsu, Jim Hsu and Wei-Yang Chou*

A novel polyimide electret using as the gate dielectric layer and charge trapping layer of *n*-type organic transistors was synthesized to improve the memory effect and electrical stability.